FUZZY SUPPORT VECTOR REGRESSION MODEL FOR THE CALCULATION OF THE COLLAPSE MOMENT FOR WALL-THINNED PIPES

HEON YOUNG YANG, MAN GYUN NA*, and JIN WEON KIM
Department of Nuclear Engineering, Chosun University
375 Seosuk-dong, Dong-gu, Gwangju 501-759, Korea
*Corresponding author. E-mail : magyna@chosun.ac.kr

Received May 11, 2008
Accepted for Publication July 14, 2008

Since pipes with wall-thinning defects can collapse at fluid pressure that are lower than expected, the collapse moment of wall-thinned pipes should be determined accurately for the safety of nuclear power plants. Wall-thinning defects, which are mostly found in pipe bends and elbows, are mainly caused by flow-accelerated corrosion. This lowers the failure pressure, load-carrying capacity, deformation ability, and fatigue resistance of pipe bends and elbows. This paper offers a support vector regression (SVR) model further enhanced with a fuzzy algorithm for calculation of the collapse moment and for evaluating the integrity of wall-thinned piping systems. The fuzzy support vector regression (FSVR) model is applied to numerical data obtained from finite element analyses of piping systems with wall-thinning defects. In this paper, three FSVR models are developed, respectively, for three data sets divided into extrados, intrados, and crown defects corresponding to three different defect locations. It is known that FSVR models are sufficiently accurate for an integrity evaluation of piping systems from laser or ultrasonic measurements of wall-thinning defects.

KEYWORDS : Collapse Moment, Fuzzy Support Vector Regression, Wall-Thinning Defect

1. INTRODUCTION

Piping systems of nuclear power plants are subject to a number of collapsing forces. In particular, the wall-thinning degradation in bent piping systems (pipe bends and elbows) of carbon steel material is considered as an important degradation factor [1]. The wall-thinning defect is mainly caused by flow-accelerated corrosion, which reduces the failure pressure, load-carrying capacity, deformation ability, and fatigue resistance of pipe bends and elbows. Therefore, it is necessary to calculate collapse loads of wall-thinned bends and elbows accurately according to defect size under various loading conditions.

Pipe bends and elbows are connected into piping systems to allow modification of the isometric routing and, more importantly, pipe bends are usually incorporated to reduce anchor reaction forces. They are also capable of absorbing considerably large thermal expansion and seismic movement through energy dissipation as a result of local plastic deformation so that they maintain the integrity of the entire piping system under transient loading conditions [2-3]. As they are regarded as critical components of nuclear power plant piping, significant care must be taken so as not to exceed their collapse moment. Therefore, as mentioned above it is essential to assess the safety margin under various operating conditions.

This paper uses a support vector regression (SVR) model [4] which has been successfully employed to solve nonlinear regression problems [5-8]. The concept of the SVR is to map nonlinearly the input data into a high-dimensional feature space and subsequently carry out linear regression. In this paper, the SVR concept is further expanded and the SVR is combined with a fuzzy algorithm in what is termed a fuzzy support vector regression (FSVR). That is, a fuzzy membership grade is applied to each data point and the SVR is reformulated so that each input data point can make different contribution to the learning of the regression function. This methodology was applied to the development of a soft-sensing model for the feedwater flowrate [9] and was shown to have good performance. The objective of the present study is to calculate the collapse moment under a variety of loading conditions for the measured defect geometry using FSVR models.

The collapse moment-related data should be provided to develop and test the FSVR model. These data are

generated [8] by performing finite element analyses (FEAs) for various loading conditions and defect geometries such as the thinning defect locations, bend radius, bend angle, wall thickness at the thinning defect, thinning length, thinning angle, internal pressure, and the closing and opening bending modes. The collapse moment is calculated using these loading conditions and defect geometries as the inputs into the FSVR models.

2. COLLAPSE MOMENT DATA USING FEAS

This study uses the collapse moment calculated using the twice-elastic slope method [10-11]. Carbon steel bends that have an outer diameter (D_o) of 400mm and a nominal thickness (t_{nom}) of 20mm are used. The bend angles (ϕ) are 30°, 60°, and 90° and the bend radius ratios (R_b/R_m) are 3 and 6, as shown in Fig. 1 [8]. Bends and elbows are connected to straight pipes with lengths equal to ten times the mean radius (R_m) to allow free ovalization of the end section of the bends. Wall-thinning defects are located at the intrados and extrados centerlines and the crown of the pipe bends and elbows; the axial and circumferential shapes of defects are circular.

The deformation behavior of an elbow under a bending load is governed by its geometry, including its bend radius, bend angle, and radius/thickness (R/t). Thus, the collapse behavior of local wall-thinned elbow is also influenced by these geometrical parameters. The R/t of an elbow is dependent on the safety class and operating pressure of the piping system, and elbows with R/t values of 10 to 30 are typically used in the secondary piping system of a NPP at which the local wall-thinning is more likely to occur. As the present results were developed based on the analysis results of an elbow when R/t=10, the results are properly applicable to the evaluation of wall-thinned elbows in a secondary piping system operated at a relatively high pressure, i.e., a high-energy piping system. Moreover, an additional analysis and verification considering various R/t values are needed to expand the applicability of present results to integrity evaluations of wall-thinned elbows operated at moderate and low pressure.

In order to evaluate the collapse moment of wall-thinned pipe bends, a nonlinear three-dimensional (3D) FEA was performed. In the FEA, various loading conditions and defect geometries were considered, as summarized in Table 1. The combined internal pressure and bending loads are considered as an applied load. A range of internal pressure from 0 to 20MPa was used, and the in-plane bending of either the closing- or opening-mode is applied at a constant internal pressure.

Table 1. FEA Conditions for Wall-Thinned Pipe Bends [8]

Wall-thinned location of pipe bends		Extrados, Intrados, Crown
Bend radius (R_b/R_m)		3, 6
Bending angle (°)		30, 60, 90
Defect geometry	L_s/D_o	0.25, 0.5, 1.0, 1.5, 2.0
	$(t_{nom}-t_p)/t_{nom}$	0.233, 0.466, 0.699
	θ/π	0.0625, 0.125, 0.25, 0.50
Load	Bending mode	Closing, Opening
	Pressure (MPa)	0, 5, 10, 15, 20

t_p : the minimum thickness of the thinned area

L : the equivalent thinning length

θ : the circumferential half angle of the thinning defect

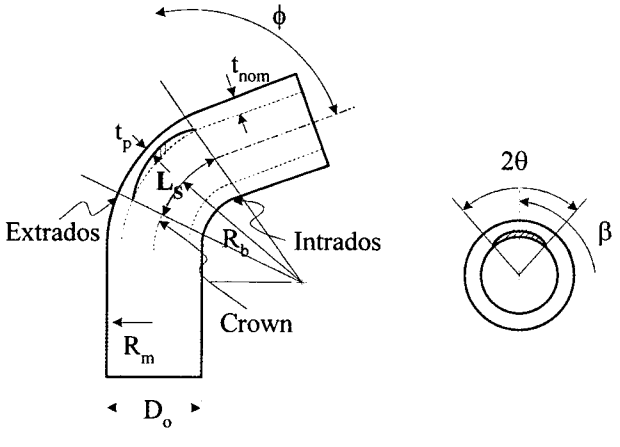

Fig. 1. Definition of Dimensions of Wall-Thinned Defects in Pipe Bends

Figure 2 depicts the finite element meshes used in the FEA. Twenty-node solid elements with a reduced integration order were used to model the bends and pipes. Considering geometrical symmetry, one fourth of the bend was modeled for both intrados and extrados wall-thinning defects, and half of the bend was modeled for a crown wall-thinning defect.

According to prior studies, the collapse moment of pipe bends and elbows with crack defects depends on the mesh patterns [10-11]. However, the gross structural behavior of defect-free pipe bends and elbows does not strongly depend on the mesh patterns [12]. Considering the characteristic of wall-thinning defects with a smooth 3D shape, as shown in Fig. 2, it is expected that the gross behavior of wall-thinned pipe bends is similar to that of defect-free pipe bends over that of cracked pipe bends. Thus, compared to the FEAs for the collapse of defect-free pipe bends [12-13], the mesh patterns used for this study are sufficient to evaluate the collapse behavior of wall-thinning pipe bends and elbows.

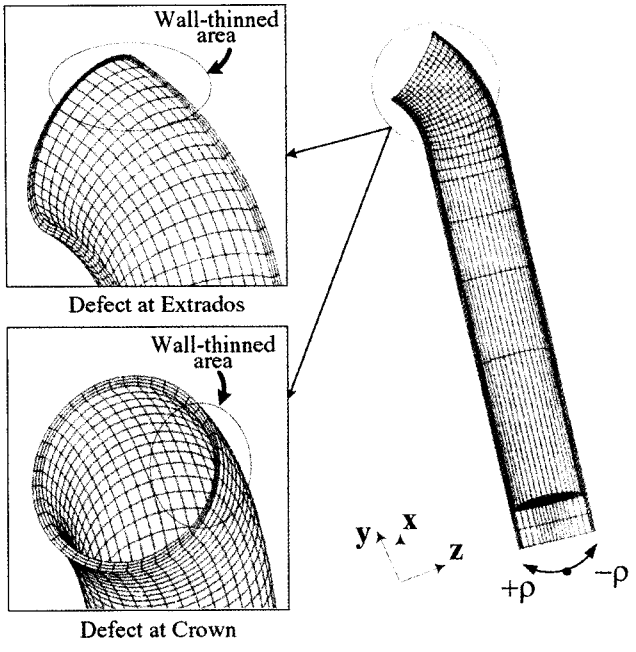

Fig. 2. Finite Element Model Used in FEAs [8]

ABAQUS code [14], a general-purpose FEA code, was used for this study. A former FEA evaluation showed that a consideration of the geometrical nonlinearity in the FEA is very important for a precise determination of a pipe bend deflection under various combinations of the closing and opening mode of bending and internal pressure [12]. Therefore, both geometric and material nonlinearity are considered in this FEA. The yield stress and ultimate tensile stress of the specific material of the bend and the attached pipes are 302MPa and 450MPa, and the elastic modulus and the Poisson ratio are 206GPa and 0.3, respectively.

3. FSVR MODELS

The SVR represents an excellent learning technique that has been introduced in the framework of structural risk minimization (SRM). Unlike classical adaptation algorithms that minimize the absolute value of the error or the mean square error, the SVR method accomplishes SRM. This way, it creates a regression model with the expected probability of error for regression problems, which implies that it provides good performance with unseen data. This property indicates that SVR models perform well on a test data set as well as on a training data set [15].

3.1 FSVR Methodology

In general regression problems, the learning machine is supplied with the training data, from which it attempts to learn the input-output relationship. The basic concept of the SVR is to map nonlinearly the original data $\mathbf{x}$ into a higher dimensional feature space. Hence, given a set of data $\{(\mathbf{x}_i, y_i)\}_{i=1}^{N}$ where $\mathbf{x}_i$ is the input vector, y_i is the actual output value and N is the total number of data points, the SVR function considers approximation functions as follows:

$$y = f(\mathbf{x}) = \sum_{i=1}^{N} w_i \phi_i(\mathbf{x}) = \mathbf{w}^T \boldsymbol{\varphi}(\mathbf{x}) + b \tag{1}$$

Here, $\phi_i(\mathbf{x})$ is a feature that is nonlinearly mapped from the input space $\mathbf{x}$, $\mathbf{w}=[w_1\ w_2\ \ldots\ w_N]^T$, and $\boldsymbol{\varphi}=[\phi_1\ \phi_2\ \ldots\ \phi_N]^T$.

The support vector weight $\mathbf{w}$ and bias b are calculated by minimizing the regularized risk function

$$R(\mathbf{w}) = \frac{1}{2}\mathbf{w}^T\mathbf{w} + \lambda \sum_{i=1}^{N} |y_i - f(\mathbf{x})|_\varepsilon , \tag{2}$$

where

$$|y_i - f(\mathbf{x})|_\varepsilon = \begin{cases} 0, & |y_i - f(\mathbf{x})| < \varepsilon \\ |y_i - f(\mathbf{x})| - \varepsilon, & \text{otherwise} \end{cases} \tag{3}$$

Here, λ and ε are user-specified parameters, and $|y_i - f(\mathbf{x})|_\varepsilon$ is the ε-insensitive loss function [4]. The loss is equal to zero if the difference between the calculated $f(\mathbf{x})$ and the measured value is less than the error level ε. Vapnik's ε-insensitive loss function defines the ε tube (see Fig. 3). If the calculated value is within the tube, the loss is zero. Here, when ε=0, Vapnik's ε-insensitive loss function is equivalent to the absolute error (L_1 norm) function. The constant λ determines the trade-off between the flatness of $f(\mathbf{x})$ (the weight vector norm) and the amount up to which deviations larger than ε are tolerated.

The FSVR is known as support vector regression (SVR) further enhanced with a fuzzy approach. The FSVR model incorporates fuzziness into the SVR model input. The

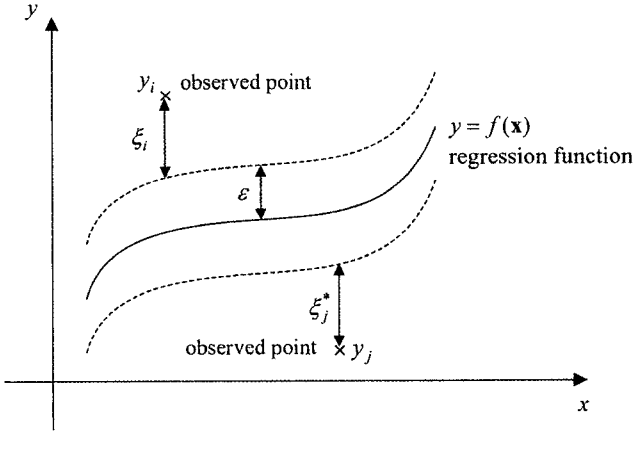

Fig. 3. The Insensitive Tube ($\pm\varepsilon$) and Slack Variables ξ and ξ^* for FSVR

proposed FSVR enhances the SVR by reducing outliers and noise. By applying a fuzzy membership function to each data point of the SVR model, the regularized risk function can be reformulated such that different input data points can make a different contribution to the learning of the regression function as follows:

$$R(\mathbf{w}) = \frac{1}{2}\mathbf{w}^T\mathbf{w} + \lambda\sum_{i=1}^{N}\mu_i\left|y_i - f(\mathbf{x})\right|_\varepsilon \tag{4}$$

Here, μ_i is a fuzzy membership grade. Common SVR methods apply an equal weight to all data points. However, the FSVR uses different weights according to their importance, as specified by the fuzzy membership grade. The regularized risk function is converted into the following constrained risk function:

$$R(\mathbf{w},\xi,\xi^*) = \frac{1}{2}\mathbf{w}^T\mathbf{w} + \lambda\sum_{i=1}^{N}\mu_i\left(\xi_i + \xi_i^*\right), \tag{5}$$

$$\text{under constraints}\begin{cases} y_i - \mathbf{w}^T\boldsymbol{\varphi}(\mathbf{x}) - b \le \varepsilon + \xi_i, & i = 1, 2, \cdots, N \\ \mathbf{w}^T\boldsymbol{\varphi}(\mathbf{x}) + b - y_i \le \varepsilon + \xi_i^*, & i = 1, 2, \cdots, N \\ \xi_i,\ \xi_i^* \ge 0, & i = 1, 2, \cdots, N \end{cases} \tag{6}$$

where $\boldsymbol{\xi}=[\xi_1\ \xi_2\ \ldots\ \xi_N]^T$ and $\boldsymbol{\xi}^*=[\xi^*_1\ \xi^*_2\ \ldots\ \xi^*_N]^T$ are slack variables representing the upper and the lower constraints on the system outputs, respectively. These slack variables have positive values.

The solution to the constrained optimization problem is given by the saddle point of the Lagrange functional:

$$\begin{aligned}&\Phi\left(\mathbf{w}, b, \xi_i, \xi_i^*, \alpha_i, \alpha_i^*, \beta_i, \beta_i^*\right) = \\ &\frac{1}{2}\mathbf{w}^T\mathbf{w} + \lambda\sum_{i=1}^{N}\mu_i\left(\xi_i + \xi_i^*\right) - \sum_{i=1}^{N}\alpha_i\left[\mathbf{w}^T\boldsymbol{\varphi}(\mathbf{x}_i) + b - y_i + \varepsilon + \xi_i\right] \\ &- \sum_{i=1}^{N}\alpha_i^*\left[y_i - \mathbf{w}^T\boldsymbol{\varphi}(\mathbf{x}_i) - b + \varepsilon + \xi_i^*\right] - \sum_{i=1}^{N}\left(\beta_i\xi_i + \beta_i^*\xi_i^*\right).\end{aligned} \tag{7}$$

The above equation is minimized with respect to the primal variables $\mathbf{w}$, b, ξ_i, ξ^*_i, and then maximized with respect to the nonnegative Lagrangian multipliers α_i, α^*_i, β_i, β^*_i. The minimum with respect to $\mathbf{w}$, b, ξ_i, ξ^*_i of the Lagrange functional gives the following conditions:

$$\begin{aligned}&\mathbf{w} = \sum_{i=1}^{N}\left(\alpha_i - \alpha_i^*\right)\boldsymbol{\varphi}(\mathbf{x}_i), \quad \sum_{i=1}^{N}\left(\alpha_i - \alpha_i^*\right) = 0, \\ &\lambda\mu_i - \alpha_i - \beta_i = 0, \quad i = 1, 2, \cdots, N, \\ &\lambda\mu_i - \alpha_i^* - \beta_i^* = 0, \quad i = 1, 2, \cdots, N.\end{aligned} \tag{8}$$

The Lagrange functional can be rewritten using the above minimum conditions, as follows:

$$\begin{aligned}\Psi\left(\alpha_i, \alpha_i^*\right) = &\sum_{i=1}^{N} y_i\left(\alpha_i - \alpha_i^*\right) - \varepsilon\sum_{i=1}^{N}\left(\alpha_i + \alpha_i^*\right) \\ &- \frac{1}{2}\sum_{i=1}^{N}\sum_{j=1}^{N}\left(\alpha_i - \alpha_i^*\right)\left(\alpha_j - \alpha_j^*\right)\boldsymbol{\varphi}^T(\mathbf{x}_i)\boldsymbol{\varphi}(\mathbf{x}_j),\end{aligned} \tag{9}$$

$$\text{under constraints}\begin{cases} \sum_{i=1}^{N}\left(\alpha_i - \alpha_i^*\right) = 0 \\ 0 \le \alpha_i \le \lambda\mu_i, \quad i = 1, 2, \cdots, N \\ 0 \le \alpha_i^* \le \lambda\mu_i, \quad i = 1, 2, \cdots, N \end{cases} \tag{10}$$

By solving the above equation using a standard quadratic programming technique, the values of α_i and α^*_i can be determined. By substituting Eq. (8) into Eq. (1), the regression function becomes:

$$y = f(\mathbf{x}) = \sum_{i=1}^{N}\left(\alpha_i - \alpha_i^*\right)\boldsymbol{\varphi}^T(\mathbf{x}_i)\boldsymbol{\varphi}(\mathbf{x}) + b = \sum_{i=1}^{N}\left(\alpha_i - \alpha_i^*\right)K(\mathbf{x}, \mathbf{x}_i) + b, \tag{11}$$

where $K(\mathbf{x},\mathbf{x}_i)=\boldsymbol{\varphi}^T(\mathbf{x}_i)\boldsymbol{\varphi}(\mathbf{x})$ is the kernel function. The kernel function used in this study is the radial basis function

$$K(\mathbf{x}, \mathbf{x}_i) = \exp\left(-\frac{(\mathbf{x} - \mathbf{x}_i)^T(\mathbf{x} - \mathbf{x}_i)}{2\sigma^2}\right).$$

Many coefficients (α_i-α^*_i) have nonzero values. The training data points corresponding to nonzero values have an approximation error equal to or larger than ε and are known as support vectors. The bias b is calculated as

$$b = -\frac{1}{2}\sum_{i=1}^{N}\left(\alpha_i - \alpha_i^*\right)\left(K(\mathbf{x}_r, \mathbf{x}_i) + K(\mathbf{x}_s, \mathbf{x}_i)\right), \tag{12}$$

where $\mathbf{x}_r$ and $\mathbf{x}_s$ are support vectors.

The two most relevant design parameters for the FSVR model are the insensitivity zone ε and the regularization parameter λ. An increase of the constant λ penalizes larger errors, which leads to a decrease of the approximation error. This can be also achieved simply by increasing the weights vector norm. However, an increase in the weight vector norm does not ensure the good generalization of a model. An increase in the insensitivity zone ε implies a reduction in the requirements for the accuracy of approximation and also decreases the number of support vectors, leading to data compression. In addition, an increase in the insensitivity zone ε has a smoothing effect on modeling data with a high noise level.

3.2 Training Data Selection

Each set of data was divided into three types of data sets: training data, optimization data, and test data. The training data set was used to solve the coefficients α_i-α^*_i, and the bias b in Eq. (11). The optimization data was used to optimize the design parameters of the FSVR models using a genetic algorithm. Test data was used for independent verification of the developed FSVR models.

The appropriate selection of training data is very important because it can affect the optimization of the FSVR model. The input and output training data is expected to have many clusters in each group and the data at these cluster centers is more informative than the neighboring data. An FSVR model for each data group (extrados, intrados, and crown defects) can be well trained using informative data. Cluster centers were located using a subtractive clustering (SC) scheme and were used as training data.

N input/output training data $\mathbf{z}_k=(\mathbf{x}_k,y_k),k=1,2,...,N$ in a group was assumed to be available and the data points were normalized in each dimension. The SC scheme begins by generating a number of clusters in $m \times N$ dimensional input space. The SC scheme uses a measure of the potential of each data point, which is a function of the Euclidean distances to all other input data points [16]:

$$P_1(k)=\sum_{j=1}^{N} e^{-4\|\mathbf{x}_k-\mathbf{x}_j\|^2/r_a^2}, \quad k=1,2,...,N. \tag{13}$$

Here, r_a is a radius that defines a particular neighborhood. It should be noted that the potential of a data point is high when it is surrounded by an abundance of neighboring data. After the potential of each data point is calculated, the data point with the highest potential is selected as the first cluster center.

In general, after determining the i-th cluster center $\mathbf{c}_i$ and its potential value P_i^c, the potential of each data point is revised using the equation

$$P_{i+1}(k)=P_i(k)-P_i^c e^{-4\|\mathbf{x}_k-\mathbf{c}_i\|^2/r_\beta^2}, \quad k=1,2,...,N, \tag{14}$$

where r_β is usually greater than r_a in order to limit the number of clusters generated. Equation (14) signifies that the amount of potential is subtracted from each data point as a function of its distance from the cluster center. The data points near the cluster center have a greatly reduced potential and are unlikely to be selected as the next cluster center. When the potentials of all data points have been revised according to Eq. (14), the data point with the highest potential is selected as the $(i+1)^{th}$ cluster center. The calculation stops when a condition, $P_i^c<\varepsilon P_1^c$, is true; otherwise the loop is repeated. If the calculation stops finally at the step N_c, there are N_c cluster centers considered to be in the data group. The input/output data (training data) positioned in the cluster centers of the data group are selected to train the FSVR model for each group. In addition, every five time-steps, the test data is selected from the remaining data where the training data had already been eliminated. Hence, the optimization data and test data comprise 80% and 20% of the remaining data, respectively.

The cluster centers selected as a training data point are more important and should be more heavily weighted relative to the other neighboring data points when training the FSAR models. Therefore, the potential of the cluster centers calculated by Eq. (13) was used as a fuzzy membership grade in Eq. (4), as follows:

$$\mu_i=1-\frac{1}{P_1(i)}, \quad i=1,\cdots,N_c. \tag{15}$$

3.3 Optimization Using Genetic Algorithm

The FSVR model is developed by learning from experimental data and should be optimized to maximize the estimation performance. The parameters to be optimized consist of the insensitivity zone ε, the regularization parameter λ, and the kernel function parameter σ for the design parameters of FSVR models; they consist of cluster radii, r_a and r_β, for the sampling of the training data.

In this study, a genetic algorithm is used to optimize the design parameters of the FSVR models. Compared to conventional optimization methods that move from one point to another, genetic algorithms start from many points, simultaneously climbing many peaks in parallel. Accordingly, genetic algorithms are less susceptible to being stuck at local minima compared to conventional search methods [17-18]. Moreover, a genetic algorithm is most useful for solving optimization problems with multiple objectives. The term *chromosome* in a genetic algorithm includes a candidate solution that minimizes an objective function, generally encoded as a bit string. As the genetic algorithm optimizes five parameters, each chromosome has five parameters encoded as a bit string. As generation proceeds, populations of chromosomes are iteratively altered by biological mechanisms inspired by natural evolution, such as selection, crossover, and mutation.

The genetic algorithms require a fitness function that assigns a score to each chromosome (candidate solution) in the current population, and maximize the fitness function value. The fitness function evaluates the extent to which each candidate solution is suitable for the specified objectives. In this study, the specified multiple objectives are to minimize the root mean square error and the maximum error by as much as possible. Therefore, the following fitness function is suggested:

$$F=\exp\left(-\mu_1 E_1-\mu_2 E_2-\mu_3 E_3-\mu_4 E_4\right). \tag{16}$$

Here, μ_1, μ_2, μ_3 and μ_4 are the weighting coefficients, and E_1, E_2, E_3 and E_4 have a concept of energy defined respectively as

$$E_1=\sqrt{\frac{1}{N_t}\sum_{k=1}^{N_t}\left(y_t(k)-\hat{y}_t(k)\right)^2}, \tag{17}$$

$$E_2=\sqrt{\frac{1}{N_o}\sum_{k=1}^{N_o}\left(y_o(k)-\hat{y}_o(k)\right)^2}, \tag{18}$$

$$E_3=\max_k\left\{y_t(k)-\hat{y}_t(k)\right\}, \text{ and} \tag{19}$$

$$E_4=\max_k\left\{y_o(k)-\hat{y}_o(k)\right\}. \tag{20}$$

The variables $y(k)$ and $\hat{y}(k)$ represent the output calculated by the FEA and the output calculated by the FSVR model, respectively. The subscripts t and o indicate the training data and the optimization data, respectively, and N_t and N_o represent the numbers of the training data and the optimization data.

4. APPLICATION TO THE CALCULATION OF THE COLLAPSE MOMENT

To develop FSVR models for calculating the collapse moment of wall-thinned pipe bends and elbows, first of all, the necessary data must be available. As sufficient related field data from nuclear power plants do not exist, FEA data were used to develop an FSVR model for each loading condition and defect geometry case, as described

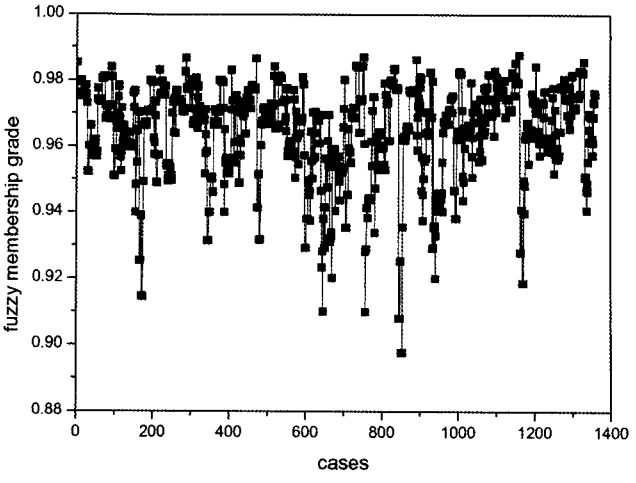

Fig. 5. Fuzzy Membership Grade of the Training Data for Extrados Defects

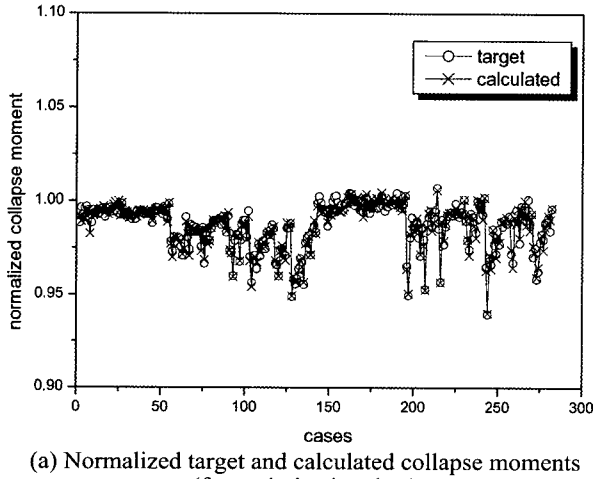

(a) Normalized target and calculated collapse moments (for optimization data)

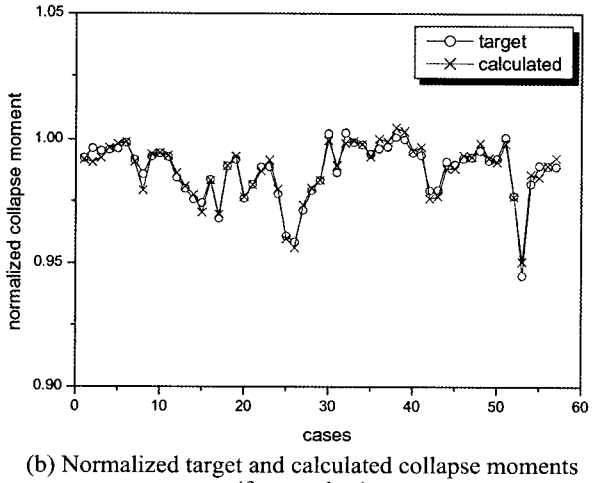

(b) Normalized target and calculated collapse moments (for test data)

Fig. 4. Performance of the FSVR Models for Extrados Defects

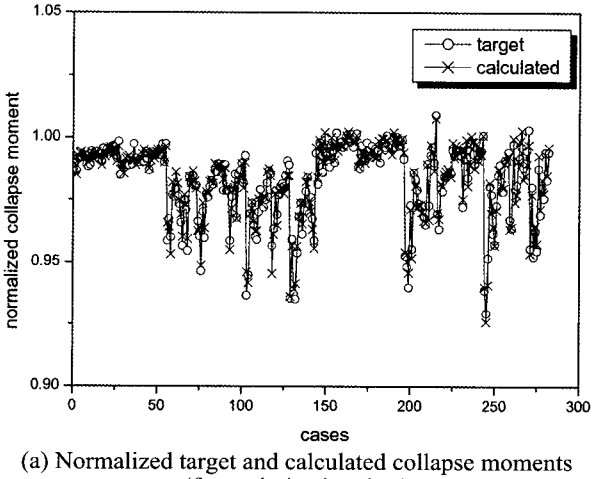

(a) Normalized target and calculated collapse moments (for optimization data)

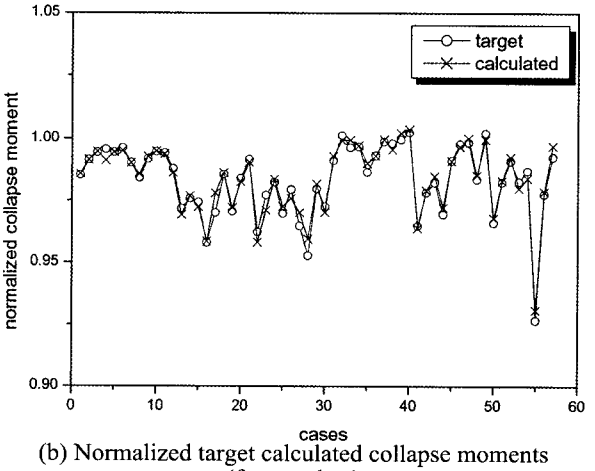

(b) Normalized target calculated collapse moments (for test data)

Fig. 6. Performance of the FSVR Models for Intrados Defects

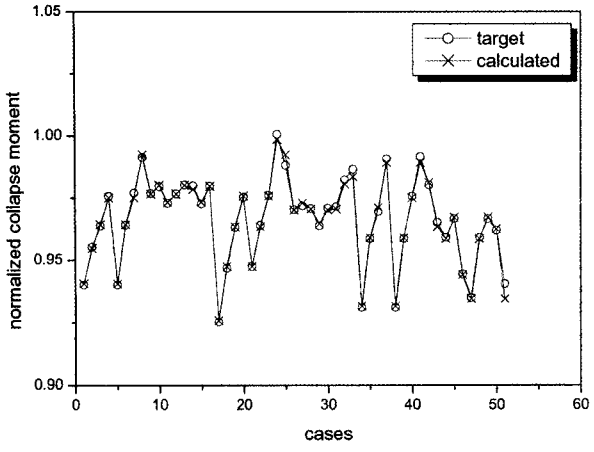

(a) Normalized target and calculated collapse moments (for optimization data)

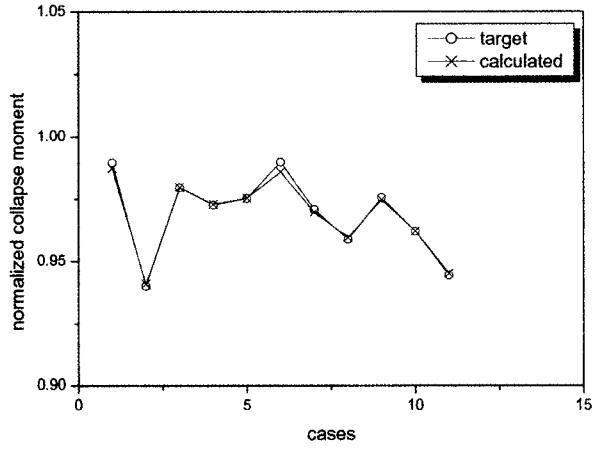

(b) Normalized target and calculated collapse moments (for test data)

Fig. 7. Performance of the FSVR Models for Crown Defects

in Section 2.

The ranges of the input signals for the FSVR models in this paper are described in Table 1. The generated data total 3712 input-output data pairs $(x_1,x_2,\cdots,x_8,y)$ consisting of 1700 extrados defect data, 1700 intrados defect data, and 312 crown defect data pairs. The characteristic of the collapse moment is much different according to the three wall-thinning defect locations of extrados, intrados, and crown, as represented by x_1. Therefore, the data are classified according to the three defect locations and three FSVR models are designed respectively for the three classes. The input signals, x_2 through x_8, indicate the bend radius, bend angle, wall thickness at the thinning defect, thinning length, thinning angle, internal pressure, and bending modes of closing and opening, respectively. The output y is the collapse moment. The inputs and output to the FSVR models are normalized so that they have a standard deviation of one and a mean of zero. The normalized input and output signals are applied to the FSVR models. The actual calculated collapse moment can easily be recovered from the normalized calculated collapse moment using the average value and standard deviation of the collapse moment of the training data.

Figure 4 shows the calculation results of the collapse moment using the FSVR model for extrados defects, intrados defects, and crown defects. Figure 5 shows the fuzzy membership values of training data inputs for the extrados defects. Figures 6-7 show the calculation results of the collapse moment using the FSVR model for intrados defects and crown defects.

Table 2 summaries the calculation accuracy of collapse moments using the FSVR models. The FSVR models show similar performance for the three defect locations. The relative RMS errors are 0.2074% for the

Table 2. Calculation Accuracy of the FSVR Models

Defect location		Extrados		Intrados		Crown		Total	
Training data selection		SC	Fixed interval	SC	Fixed interval	SC	Fixed interval	SC	Fixed interval
Fitness		0.9288	0.1359	0.8995	0.1943	0.9678	0.8264	-	-
Number (No.) of SVs		947	904	741	1000	205	227	1893	2131
Training data	No. of data	1361	1361	1361	1361	250	250	2972	2972
	RMS error (%)	0.2098	0.3274	0.2205	0.0987	0.0849	0.2304	**0.2074**	0.2409
	Max error (%)	2.8201	4.5267	0.3860	0.1589	0.1022	2.4363	2.8201	4.5267
Optimization data	No. of data	282	282	282	282	51	51	615	615
	RMS error (%)	0.2155	0.5391	0.3167	0.8084	0.1367	0.3822	**0.2624**	0.6671
	Max error (%)	0.8279	6.5296	1.1647	4.9616	0.5927	1.0549	1.1647	6.5296
Test data	No. of data	57	57	57	57	11	11	125	125
	RMS error (%)	0.2543	0.3312	0.2703	0.4589	0.1540	0.4081	**0.2547**	0.4009
	Max error (%)	0.6529	1.2211	0.8076	1.8703	0.4050	0.8076	1.4957	1.8703

training data, 0.2624% for the optimization data, and 0.2547% for the test data. Additionally, it is known that the RMS error magnitude of the FSVR models of the test data is similar to that of the optimization data. Therefore, if the FSVR models are optimized first using data for a variety of loading conditions and defect geometry cases, they can accurately calculate the collapse moment for any other defect case. Table 2 shows the calculation results when the training data are selected at every fixed interval in a given data set. As shown in Table 2, the FSVR model with the SC data sampling option is much better than that with a fixed interval sampling. The collapse moment calculation was done in a previous study [8] using the SVR models. However, it is shown in this paper that FSVR models can calculate the collapse moment more accurately. In the aforementioned previous study, even if the training data, the optimization data, and the test data differ from those of the present study, the relative RMS errors are 0.2333% for the training data, 0.5229% for the optimization data, and 0.5011% for the test data. Considering that the calculation accuracy of test data is most important, (i.e., considering the RMS errors of the test data set), the calculation accuracy of the proposed method is approximately two times better compared to that of the previous study [8].

5. CONCLUSIONS

In this paper, an FSVR method is used to calculate the collapse moment due to the wall-thinning defects of bends and elbows in piping systems. Three FSVR models were developed for three data sets divided into the three classes of extrados, intrados, and crown defects. The FSVR models were trained using the data set prepared for training (training data), optimized by the optimization data set, and verified using the test data set independent of the training data and the optimization data. The developed FSVR models were applied to the numerical data obtained by the FEA. The relative RMS errors are 0.2074% for the training data, 0.2624% for the optimization data and 0.2547% for the test data. The RMS error magnitude of the FSVR models for the test data is similar to that for the optimization data. Therefore, if the FSVR models are optimized first using a number of data that include a variety of loading conditions and defect geometry cases, they can accurately calculate the collapse moment for any other defect case. Essentially, this method was developed to predict the collapse moment easily for the measured defect geometry.

REFERENCES

[1] B. Chexal, J. Horowitz, B. Dooley, P. Millett, C. Wood, and R. Jones, "Flow-Accelerated Corrosion in Power Plant," EPRI/TR-106611-R2 (1998).

[2] V. C. Martzen and L. Yu, "Elbow Stress Indices using Finite Element Analysis," *Nucl. Eng. & Des.*, **181**, 257 (1998).

[3] M. A. Shalaby and M. Y. A. Younan, "Limit Loads for Pipe Elbows Subjected to In-Plane Opening Moments and Internal Pressure," *J. Press. Ves. Tech.*, **121**, 17 (1999).

[4] V. Vapnik, *The Nature of Statistical Learning Theory*, Springer, New York (1995).

[5] A. Kulkarni, V. K. Jayaraman, and B. D. Kulkarni, "Control of Chaotic Dynamical Systems Using Support Vector Machines," *Physics Letters A*, **317**, 429 (2003).

[6] P. -F. Pai and W. -C. Hong, "Support Vector Machines with Simulated Annealing Algorithms in Electricity Load Forecasting," *Energy Conversion and Management*, **46**, 2669 (2005).

[7] W. Yan, H. Shao, and X. Wang, "Soft Sensing Modeling Based on Support Vector Machine and Bayesian Model Selection," *Computers and Chemical Engineering*, **28**, 1489 (2004).

[8] M. G. Na, J. W. Kim, and I. J. Hwang, "Collapse Moment Estimation by Support Vector Machines for Wall-Thinned Pipe Bends and Elbows," *Nucl. Eng. Des.*, **237**, 451 (2007).

[9] M. G. Na, H. Y. Yang, and D. H. Lim, "A Soft-Sensing Model for Feedwater Flow Rate Using Fuzzy Support Vector Regression," *Nucl. Eng. Tech.* **40**, 69 (2008).

[10] K. Yahiaoui, D. G. Moffat, and D. N. Moreton, "Piping Elbows with Cracks, Part 2: A Parametric Study of the Influence of Crack Size on Limit Loads due to Pressure and Opening Bending," *J. Strain Anal.*, **35**, 35 (2000).

[11] K. Yahiaoui, D. G. Moffat, and D. N. Moreton, "Piping Elbows with Cracks, Part 2: Global Finite Element and Experimental Plastic Loads under Opening Bending," *J. Strain Anal.*, **35**, 47 (2000).

[12] J. Chattopadhyay, "The Effect of Internal Pressure on In-Plane Collapse Moment of Elbows," *Nucl. Eng. Des.*, **202**, 133 (2002).

[13] A. Robertson, H. Li, and D. Mackenzie, "Plastic Collapse of Pipe Bends under Combined Internal Pressure and In-Plane Bending," *Int. J. Pres. Ves. & Piping*, **82**, 407 (2005).

[14] H. D. Hibbitt, B. I. Karlsson, and E. P. Sorensen, "ABAQUS/Standard User's Manual," Hibbitt, Karlsson & Sorensen, Inc., Pawtucket, RI (2001).

[15] K. Vojislav, *Learning and Soft Computing – Support Vector Machines, Neural Networks and Fuzzy Logic Models*, The MIT Press, Cambridge, MA (2001).

[16] S. L. Chiu, "Fuzzy Model Identification Based on Cluster Estimation," *J. Intell. Fuzzy Systems*, **2**, 267 (1994).

[17] D. E. Goldberg, *Genetic Algorithms in Search, Optimization and Machine Learning*, Addison Wesley, Reading, MA (1989).

[18] M. Mitchell, *An Introduction to Genetic Algorithms*, The MIT Press, Cambridge, MA (1996).